International Journal of Engineering Research and Development
e-ISSN: 2278-067X, **p**-ISSN : 2278-800X, www.ijerd.com
Volume 5, Issue 8 (January 2013), PP. 09-18

X-Ray Analysis and Dielectric Characterization of Bismuth Layered (Bi_2O_3) ($Ba_xfe_{1-X}o_3$) Nanocrystalline Ceramic

Paramjeet Singh[1], A. Agarwal[2], S. Sanghi[3],Ravish Garg[4], Sonia Chhikara5
Department of Applied physics, Guru Jambheshwar University of Science & Technology, Hisar-125001, Haryana, India.
Department of Biomedical Engineering, Guru Jambheshwar University of Science & Technology, Hisar-125001, Haryana, India.
Maharishi Dayanand University, Rohtak, Haryana,India.

Abstract:- Polycrystalline ceramics of bismuth layered structure of $(Bi_2O_3)(Ba_xFe_{1-x}O_3)$ ($0.2 \leq x \leq 0.8$, x is in step of 0.2) have been prepared by conventional solid-state reaction method to study its modified dielectric and electrical properties. X-ray diffraction technique is used on the powdered samples for physical characterization and an average grain size of 16 – 21 nm was obtained. The XRD analysis reveals the single phase structure of the sample. Dielectric properties, viz, dielectric constant (ε′), dielectric loss (tan δ) and ac electrical conductivity of the ceramic sintered at various temperatures have been studied in the frequency range 10^{-1}-10^{7} Hz. The frequency and temperature dependent conductivity investigations have been carried out by using impedance spectroscopy. It was observed that the sample exhibit bulk conduction which increase with increase in temperature and with the increase in barium (Ba) concentration. The conductivity mechanism at room temperature shows a frequency dependence, which can be ascribed due to the presence of oxygen vacancies. Combined impedance and modulus plots were used to analyze the sample behavior as a function of frequency and temperature. The effect of temperature on the scaling of dielectric modulus indicates that the conductivity relaxation mechanism is temperature independent. The overlapping of the normalized peaks corresponding to impedance and electrical modulus suggests the single mechanism for the dynamic processes occurring in the present ceramics. The dielectric and conductivity properties of this ferroelectric ceramic make it a promising material for fatigue resistance in device applications.

Keywords:-Bismuth layered structure ferroelectrics (BLSF), solid-state reaction method, Debye relaxation, Impedance spectroscopy

I. INTRODUCTION

Bismuth layered structured ferroelectrics (BLSF) compounds belongs to the Aurivillius family having perovskite like layer in between those of bismuth oxide (Bi_2O_2) layers. These compounds have a general formula $(Bi_2O_2)^{2+}(A_{m-1}B_mO_{3m+1})^{2-}$ where A is mono, di, trivalent ions or a mixture of them and B is a small sized cation with higher valences and 'n' is the number of octahedral layers. These compounds are known to be high temperature piezoelectric materials with large coercivity, high temperature stability, low dielectric loss, high anisotropy and added advantage of being lead-free unlike PZT or PLZT etc. It is found that the ferroelectric properties for even (n = 2m) and odd (n = 2m+1) aurivillius phase compounds are different. The odd layer compounds show single first-order phase transition and many even layered compounds show two transitions at different temperatures. The spontaneous polarization P_s of even-layer compounds is only along the 'a' axis. The cubo-octahedral A sites and octahedral B sites of perovskite layers in these compounds can be substituted by various aliovalent ions. The $(Bi_2O_2)^{2+}$ layers are very strong and can not be easily disturbed [1, 2]. Nowadays, much research work has been found on improvement of dielectric and ferroelectric properties of bismuth layered perovskites. It is interesting to note that by doping of various metal oxides in the above bismuth compounds, physical properties of the materials can be improved. The major contribution to the ferroelectric polarization of bismuth layered perovskites is due to the displacement of A-site cations along the 'a' axis of the perovskite unit accompanied by octahedral rotation around a and c axis. Because of the presence of Fe ions, these materials not only show ferroelectric properties but also have magnetic ordering [3].The impedance spectroscopic methods are very effective tools and widely used to characterize dielectric behavior of the polycrystalline ceramic materials. The data may be analyzed in terms of four possible formalisms, the impedance Z*, the electric modulus M*, the permittivity ε *, and the admittance Y*. These are interrelated as:

$$M^* = j\omega C_0 Z^*,$$
$$\varepsilon^* = (M^*)^{-1},$$
$$Y^* = (Z^*)^{-1},$$
$$Y^* = j\omega C_0 \varepsilon^*. \quad (1)$$

Where ω is the angular frequency, C_0 is the vacuum capacitance of the measuring cell and electrodes with an air gap in place of the sample. $C_0 = \varepsilon_o / k$, where ε_o is the permittivity of free space {8.854×10^{-14} F/cm}, and k = l/A, the cell constant where l is the thickness and A is the area of the specimen, respectively. In general, the dielectric properties of ferromagnetic materials arise due to intra-grain, inter-grain and other electrode effects. Complex impedance analysis has been emerged as a very powerful tool for separating out the grain, grain boundary, and electrode contributions in the electrical properties of samples. In the present work, to elicit more information about the mechanism of electrical transport in the titled ceramic, a detailed and systematic investigation on impedance and dielectric measurements have been carried out at different frequencies and temperatures.

II. EXPERIMENTAL

The polycrystalline fine powders of $(Bi_2O_3)(Ba_xFe_{1-x}O_3)$ ceramic ($0.2 \leq x \leq 0.8$, x is in step of 0.2) were prepared from solid-state reaction technique by using analytical grade Bi_2O_3, Ba_2CO_3, Fe_2O_3 in stoichiometric ratios. The exact composition along with sample code of all the prepared ceramics is given in Table 1. The reactants were mixed and grinded mechanically. The ceramic samples were sintered in air atmosphere at optimized temperatures and time, i.e., at 850, 800, 700, and 600°C respectively, for 6 hours (to avoid melting) with a uniform increase in temperature at a rate of 1°C per minute in a programmable electric furnace. The formation of single-phase compounds was checked with an X-ray diffraction (XRD) technique on powdered samples. To study the crystal structure of the compounds at room temperature, X-ray diffraction patterns were recorded on the powdered samples in a wide range of Bragg angles '2θ' ($10° \leq 2\theta \leq 80°$) with CuK_α radiation (λ = 1.5405 Å). Requisite amount of polyvinyl alcohol (PVA) was added as a binder to make the pallets of the powdered samples. The pellets (13 mm in diameter and 1 to 3 mm in thickness) were prepared using a hydraulic press at a pressure of 15 tons. After this the pallets were heated at 500°C for one hour to remove the PVA. For dielectric measurements both the parallel surfaces of the sintered pellets were coated with high purity air-drying silver paint and then dried for 2 hours at 200°C prior to electrical measurements. Electrical measurements of the samples were carried out in a wide frequency range (10^{-1} to 10^7 Hz) at different temperatures (30°C–200°C) using a computer–controlled LCR meter/impedance analyzer. The complex dielectric constant and dielectric loss were calculated at different temperatures and different frequencies. The complex impedance data, Z*(ω), were plotted in the Nyquist representation form, a typical complex plane plot between the imaginary part Z″ (ω) and real part Z′ (ω) for each temperature. The ac conductivity was also calculated using the complex impedance data. Error in the measurement of complex impedance data was ± 1%.

III. RESULTS AND DISCUSSION

3.1. X-ray analysis

Fig.1 shows the XRD patterns of all the sintered BBFO samples. Preliminary examination of the raw X-ray powder diffraction data for all samples suggested that these powders are crystalline in nature with more than one phase.

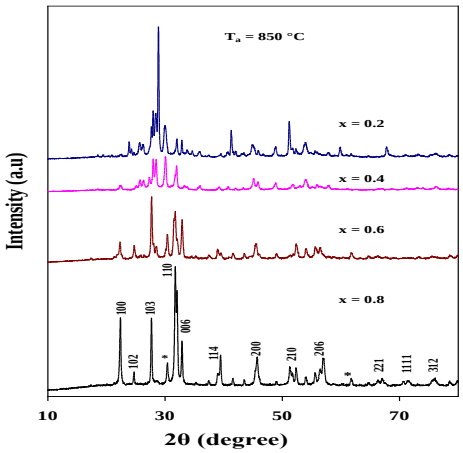

Fig.1. X-ray diffraction patterns of $(Bi_2O_3)(Ba_xFe_{1-x}O_3)$ samples (T_a = 850˚C).

The sharp and single reflection peaks were found in the reflection pattern, which are different from those of the ingredient precursors, and confirms the formation of new compounds. Also, it was observed that the intensity of major peaks increase with increase in value of 'x' which indicates the increase in crystalline nature of compounds. Also, new peaks are formed with the increased concentration of Ba ion. Lattice parameters have been calculated from the d-values obtained from XRD data. It is observed that the peaks in the pattern for x = 0.6 ceramic belongs to tetragonal primitive structure having space group P4/mmm (ICDD# 898412). However, a small variation in the position and intensity of the peaks is observed indicating a variation in the lattice parameters. All the peaks are indexed except two (shown by *), which are unidentified. The change in lattice parameter is expected on substituting bigger Ba ion (ionic radius 1.61 Å) for Fe ion (ionic radius 0.64 Å). It is observed that doped samples show an overall increase in lattice constant (Table 1) which may be due to structural constraint induced by the $(Bi_2O_2)^{2+}$ interlayer [4, 5].

Table.1

Average grain size (D) at (T_a = 700 ^oC), lattice constant(LC), dielectric constant (ε′), tangent loss (tanδ), ac conductivity(σ_{ac}), activation energies (E_a), and grain resistance (R_g) of **(**Bi_2O_3)($Ba_xFe_{1-x}O_3$**)** samples for T_a = 700^oC.

Sample code	x	D (nm)	LC Å	ε′ at (100 ^oC,10Hz)	tan δ at (100 ^oC,10Hz)	σ_{ac}(×10^{-6})(Ωm)$^{-1}$ at (100 ^oC,10Hz)	E_a (ev) E_1	E_a (ev) E_2	R_g (MΩ)
BBFO1	0.2	16	3.97	642	0.21	3.3	0.014	0.003	1.17
BBFO2	0.4	17	4.04	968	0.25	4.2	0.024	0.006	3.42
BBFO3	0.6	21	4.20	1550	0.36	9.7	0.031	0.008	7.91
BBFO4	0.8	21	4.36	2071	0.67	210	0.203	0.073	8.23

This $(Bi_2O_2)^{2+}$ layer does not allow the crystal lattice to expand at low doping concentrations. At higher doping concentration the expanding tendency of the crystal lattice overcomes the $(Bi_2O_2)^{2+}$ constraint. The average crystallite size of the samples were calculated using broadening ($\beta_{1/2}$) of a few reflection peaks at given Bragg's angle (θ) using Scherrer's equation

$$D = \frac{k\lambda}{\beta\cos\theta} \qquad (2)$$

Where k = 0.89 and λ = 1.5404 Å [6]. The calculated values of 'D', (ignoring the strain, instrumental and other effects of broadening) for the samples were found to be approximately in the range 16 – 21 nm (Table 1). Also, the average crystallite size increases slightly with doping concentration.

3.2. Dielectric properties

Lattice distortions have significant influence on the dielectric properties of bismuth layered ferroelectric materials [7, 8]. Fig. 2 shows the variation of real part of dielectric constant (ε′) with temperature at different frequencies (for BBFO4 sample, T_a = 800°C). It is observed that the dielectric constant increase with increase in temperature. This increase is quite significant at lower frequencies in comparison to higher frequencies. It is known that the dielectric constant of ceramics, in general, depends on dipolar, interfacial, ionic and electronic polarizations. Dipolar and interfacial polarizations play important role at lower frequencies and are temperature dependent. At higher frequencies, ionic and electronic polarizations contribute to the dielectric constant and are temperature independent [9]. Therefore, in present ceramics, the significant increase in dielectric constant at lower frequencies with temperature arises from the dipolar and interfacial polarizations. At higher frequencies, ε′ is almost constant due to contribution from ionic and electronic polarizations.

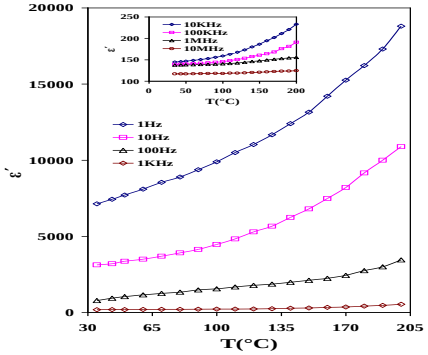

Fig.2 Variation of real part of dielectric constant (ε') with temperature at various frequencies for BBFO3 sample (T_a = 800^oC).

Fig. 3 shows the variations in dielectric constant (ε′) with frequency at different temperatures. At low frequency ε′ decreases exponentially with small increase in frequency.

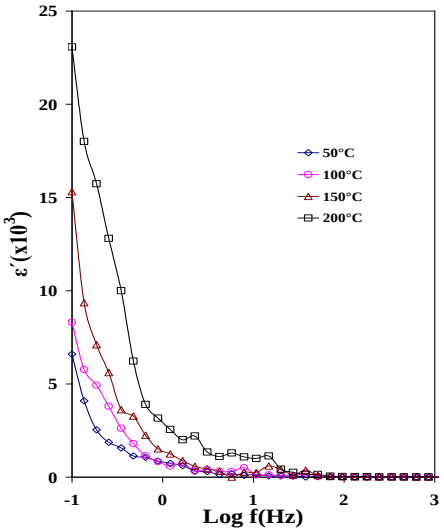

Fig.3 Variation of real part (ε') of dielectric constant with frequency at different temperatures for BBFO3 sample (T_a = 800°C).

At higher frequency, ε′(ω) approaches a constant value, ε′∞, this probably results from rapid polarization process[10]. This behavior supports the high dispersion at low frequency as shown by Fig. 2. Also, ε′(ω) increase with decrease in frequency due to electrode polarization arises usually from space charge accumulation at the electrode sample interface. The increase in ε′(ω) is more pronounced at higher temperatures and at lower frequencies. This may be due to the frequency dependent orientational polarization. At lower frequency, the dipoles align themselves along the field and contribute fully to the total polarization. At higher frequency, the variation in the field is too rapid for the dipoles to align themselves, so their contribution to the polarization and hence to dielectric permittivity can become negligible. The phase difference due to the loss of energy within a sample at a particular frequency is the loss factor tangent given by tanδ = ε″/ ε′. The temperature dependence of tanδ at different frequencies for BBFO4 sample is shown in fig. 4.

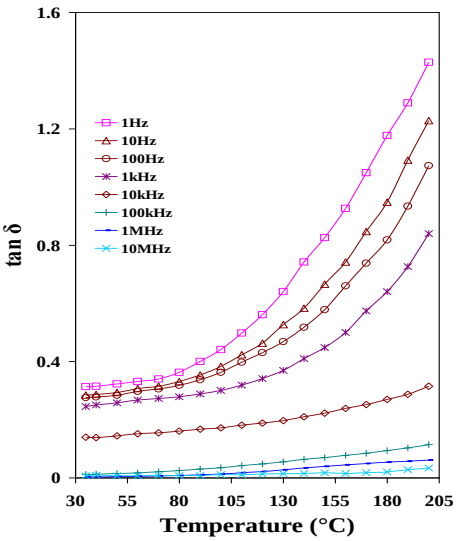

Fig.4 Temperature dependence of dielectric loss at different frequencies for BBFO3 sample (T_a = 800 ˚C).

It remains almost constant up to 100°C and then stars increasing with temperature. However, this increase is more pronounced at lower frequencies and decrease with increase in frequency. The dielectric loss factor continues to increase at higher temperature which might be attributed to the higher conductivity at higher temperature. The oxygen vacancy is a dominant defect in the layered structure perovskite materials, so the formation of higher concentration of charge carrier of oxygen vacancies and other defects all might deteriorate the conductivity. The frequency dependence of tanδ at different temperatures for BBFO4 sample is shown in fig. 5. It is observed from the figure that dielectric loss increase with increase in frequency and a peak is observed

when the hopping frequency of the ions matches with the frequency of the applied electric field. At this resonant frequency, ions hopping between adjacent sites increases rapidly, this results in increased conduction losses. With further increase in the frequency, the dielectric loss decreases and reaches a constant value as the frequency of hopping ions lags behind the frequency of applied ac field. Fig. 5 also shows that the dielectric loss versus frequency curve shows peaks and these peaks shift towards lower frequency with increase in temperature of the perovskite sample. The hopping frequency of the electrons increases with temperature and therefore the resonance occurs at lower frequency leading to a shift of loss peak toward lower frequency [11]. After the peak all curves merge together and become temperature independent.

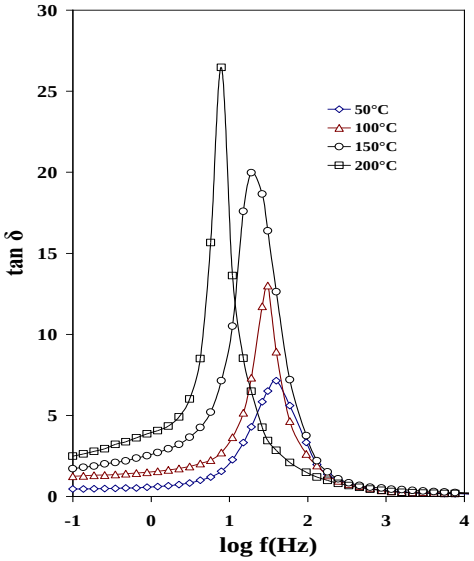

Fig.5 Variations of loss tangent (tan δ) with frequency at different temperature for BBFO3 sample.

It has also been observed that the dielectric loss increases with increase in annealing temperature of the samples because of the appearance of imperfections, increase in grain growth and conversion of Fe^{3+} ions to Fe^{2+} ions [12].

3.3. Electrical conductivity

The temperature dependence of ac conductivity at different frequencies can be calculated from the dielectric data using the relation $\sigma_{ac} = \omega\varepsilon_o\varepsilon_r\tan\delta$, where ε_r is relative dielectric constant [13, 14]. It is well known that the mechanism of electrical conduction is the same as that of dielectrical polarization. The phenomenon of conductivity dispersion in solids is generally analysed using Jonscher's power law i.e. $\sigma(\omega)= \sigma_0 + A\omega^n$, where σ_0 is the dc conductivity due to excitation of electron from a localized state to the conduction band at a particular temperature, $A\omega^n$ is the ac conductivity due to the dispersion phenomena occurring in the material, A is the temperature dependent constant and n is the temperature dependent power law exponent in range between 0 and 1 and can be calculated from the slope of log-log curve of conductivity versus frequency [15, 16]. The exponent n represents the degree of interaction between mobile ions with the lattice around them and the pre exponential factor A determines the strength of polarizability. The variation of ac conductivity with frequency is shown in Fig. 6 for BBFO3 ceramic at different temperatures.

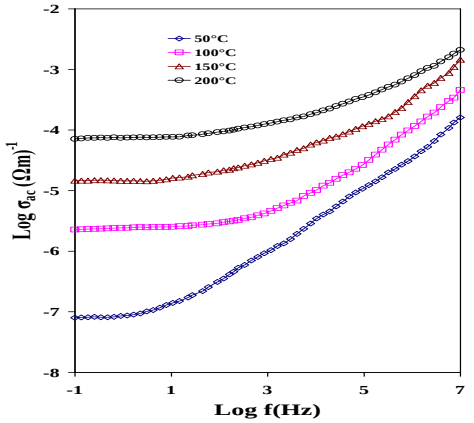

Fig.6 Variations of ac conductivity with frequency at different temperatures for BBFO3 sample.

The plots display the typical shape found for electrically conducting materials [17]. A flat dc plateau can be observed at low frequency and high temperature ranges. At lower temperatures, conductivity becomes a strong function of frequency and dc plateau is less observable in the available frequency window. In the higher frequency region, strong dispersion of electrical conductivity was observed and the changes of $\sigma(\omega)$ in this region can be described as proportional to ω^n, where ω is angular frequency and n is the temperature dependent power law exponent. The character of these changes does not depend on the temperature. Although with the increase in temperature it was noted that the range of frequency where dispersion occurs moved to higher frequencies. A similar tendency was observed for BBFO1, BBFO2, and BBFO4 samples. It was also found that the ac conductivity values decrease strongly with temperature below 180°C in the whole frequency range. The temperature dependence of σ_{ac} for various frequencies is shown in Fig. 7. The linear variation of the logarithm of conductivity with the reciprocal of temperature shows that the present samples obey the well known Arrhenius equation given by

$$\sigma_{ac} = \sigma_0 e^{(\frac{-E_a}{K_B T})} \qquad (3)$$

Where E_a is the activation energy and K_B the Boltzman constant. The activation energy (E_a) for the conduction process was calculated from the slope of the straight line portion of Fig. 7. Different slopes over the entire set of measurement are an evidence of different conduction mechanisms. The values of E_a and ac conductivity are given in Table 1. It is clear from the table that both the values of ac conductivity and activation energy E_a increase with increase in doping concentration 'x'.

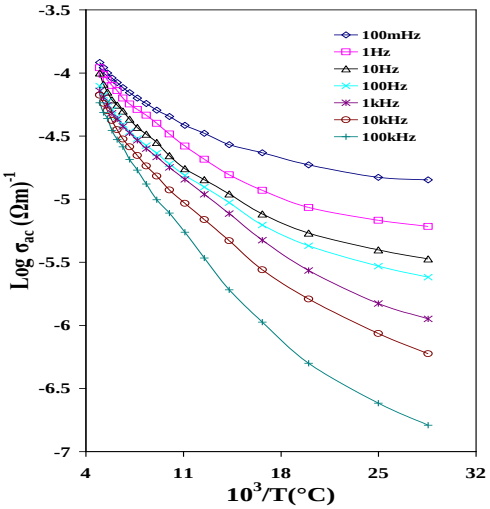

Fig. 7 Inverse temperature variations of ac conductivity at different frequencies for BBFO3 sample.

At low temperature region, the conduction mechanism is dominated by the extrinsic impurity conduction with very similar activation energy, whereas the conduction at the high temperature range is likely predominated by intrinsic defects. Increase in activation energy with doping concentration could be explained by the fact that the substitution of Ba^{2+} into the Fe^{3+} sites resulted in an enhanced stability of the perovskite structure due to the higher chemical bond strength of Ba – O bonds (562±2 KJ/mol at RT) as compared with that of Fe – O bonds (390.4± 17.2 KJ/mol at RT). For ionic conduction in oxide systems, oxygen vacancies are commonly charge carriers for both intrinsic and extrinsic conduction. Partial substitution of trivalent Fe^{3+} by divalent Ba^{2+} would introduce one extra oxygen cation which would create possible vacancies. Consequently the amount of charge carriers would be increased and thus conductivity increased with increase in Ba^{2+} ion doping.

3.4. Complex impedance analysis

Fig. 8 shows the Nyquist plots (Cole-Cole plots) at selected temperatures for BBFO4 sample. The single semicircular arc of Z'' vs. Z' plots on linear scale indicates that the transport properties of the material arise due to the bulk conduction mechanism. No residual semicircle at low frequency side has been noticed which shows the absence of contact or electrode effects. The impedance spectra of Fig. 8 can be interpreted by means of an equivalent circuit where each impedance semicircle can be represented by resister R, and capacitor C, in parallel combination corresponding equivalent to the individual component of the material i.e., bulk and grain boundary. Ideally, such semicircular arc passes through the origin of complex plot and gives a low frequency intercept on the real axis corresponding to the resistance, R of the sample [18-20]. The capacitance can be calculated by using equation

$$\omega\tau = 1 \qquad \text{i.e.,} \quad 2\pi fRC = 1 \tag{4}$$

where ω is the frequency at the maximum of the semicircle for the component.

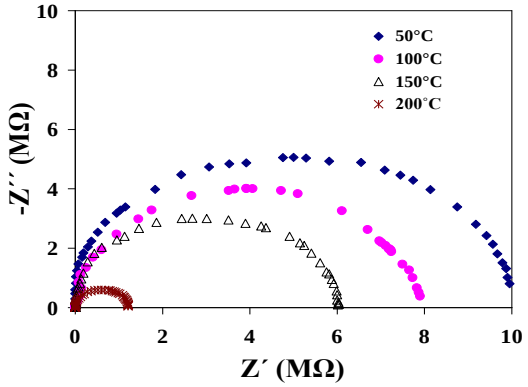

Fig. 8 Complex impedance plots at different temperatures for BBFO3 sample (T_a = 800°C).

The calculated values of R_g and C_g for all the samples are given in Table 1. The bulk resistance (dc resistance) of the samples decreases with increase in temperature as indicated by the corresponding reduction in diameters of the semicircles on increasing temperature. This is analogous to the negative temperature coefficient of resistance (NTCR) normally observed in semiconductors [21, 22]. Also the value of bulk resistance R_g increases with the increase in doping concentration of Ba^{2+} ion (Table 1). The impedance plots for all compositions comprise of a single semicircular arc with centre below the real axis, suggesting the slight departure of process from the ideal Debye behavior [23]. This departure is due to the presence of distributed elements in the material electrode system. The angle, $\theta = \frac{n\pi}{2}$ by which such a semicircular arc is depressed below the real axis, is related with the width of the relaxation time distribution and other parameters. However the source of distribution of relaxation times is the existence of inhomogeneity in the electrical conductivity and can be described in the circuits by the CPE (constant phase element).

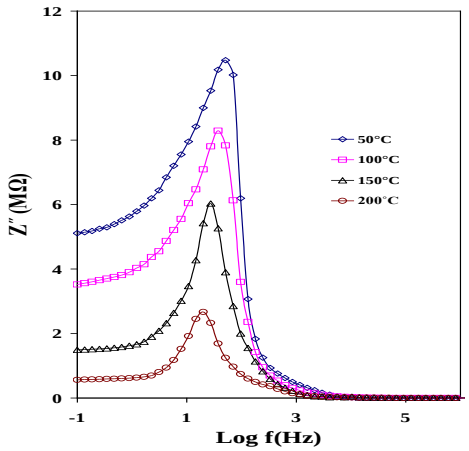

Fig. 9 Frequency dependence of imaginary part of impedance (Z″) for BBFO3 sample (T_a = 800 °C).

Fig. 9 shows the frequency dependence of the imaginary part of impedance (Z″) at different temperatures for BBFO3 ceramic (T_a = 800°C). At all temperatures studied (i.e., up to 200°C), there is a distinct sharp peak in the low frequency region which indicates a single relaxation process. The peak broadens slightly with increase in temperature suggesting that relaxation occurs over several decades of frequency. The frequency (f_o) corresponding to maximum value of Z″ (i.e., Z''_{peak}) shifts towards lower frequencies with increasing temperature which indicates the increase in relaxation time with increase in temperature. Also, it is clear from the figure that, irrespective of the temperatures at which the measurements are made, all the curves merge at higher frequencies which confirms the temperature independent behavior. At higher frequencies, the contribution from the grain predominates owing to the absence of the space charge effects. The relaxation time (τ) associated with each peak was obtained by using the equation

$$\tau = 1/2\pi f_o \tag{5}$$

The values of τ increase with increase in temperature (Table 2). A similar kind of behavior is observed in all the samples. This variation of Z″ with frequency resembles characteristics of a relaxor ferroelectric. The relaxation times considered here are the overall relaxation times depicting the average of all processes under way in the sample due to the application of ac fields.

3.5. Complex modulus analysis

The dielectric modulus model is very suitable to detect bulk effect and electrode polarization as apparent conductivity relaxation times [24-26]. The dielectric modulus is defined as

$$M^* = 1/\varepsilon^* = \frac{\varepsilon'}{\varepsilon'^2 + \varepsilon''^2} + j\frac{\varepsilon''}{\varepsilon'^2 + \varepsilon''^2} \quad (6)$$

$$= M' + jM'' \quad (7)$$

Where ε * is the complex permittivity. Fig. 10 shows the variations of real (M′) and imaginary (M″) parts of the electrical modulus as a function of frequency at different temperatures.

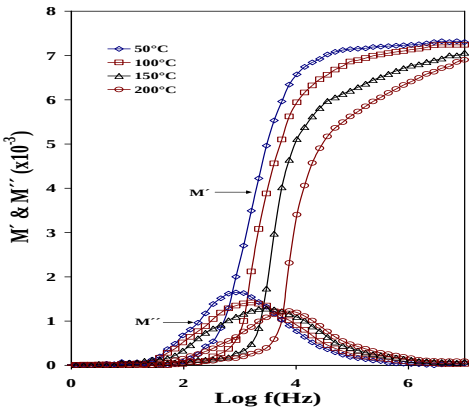

Fig. 10 Frequency dependence of the real (M′) and imaginary (M′′) parts of electric modulus at different temperatures for BBFO3 sample (T_a= 800 °C).

All the curves of imaginary part (M″) show sharp and distinct peaks. In the studied samples the peaks are quite symmetrical in a considerable frequency range at each measured temperature. The maximum in the M″ peak shifts to higher frequency with increasing temperature so, the electrode polarization effects can be avoided. These peaks indicate the transition from short range to long range mobility with decreasing frequency. The frequency region below peak maximum of M″ determines the range in which charge carriers are mobile on long distances, i.e., performing successful hoping from one sight to the neighboring site and at frequency above peak maximum of M″, the carriers are confined to potential wells, being mobile on short distances [27-30]. The frequency of the peak maxima in M″ spectroscopic plots are given by the relation

$$2\pi fRC = 1 \quad (8)$$

The RC product for each peak is a fundamental parameter as also is the value of relaxation frequency (f_{max}). This is because the RC product is usually independent of the geometry of the region responsible for the RC element [31]. The relaxation time, $\tau_{M''}$ can be obtained from the position of the maximum M″ with the following relation

$$f_{M''} = \frac{1}{2\pi\tau_{M''}} \quad (9)$$

As where $f_{M''}$ is the characteristic relaxation frequency of the peak. The value of $\tau_{M''}$ for BBFO3 sample at selected temperatures is given in Table 2.

Table 2

Relaxation time for tangent loss ($\tau_{\tan\delta}$); complex impedance ($\tau_{Z''}$); and complex modulus ($\tau_{M''}$) respectively, grain resistance (R_g) and grain capacitance (C_g) at different temperatures for BBFO3 ceramics (x = 0.6, T_a = 700°C).

T (°C)	$\tau_{\tan\delta}$ (×10^{-3})(s)	$\tau_{Z''}$ (×10^{-3})(s)		$\tau_{M''}$ (×10^{-5})(s)			R_g (MΩ)	C_g (nF)
50	4.16	3.08		18.57		10.16	0.0001	
100	5.63			4.21	9.95	7.91	0.0005	

150	9.56	5.76	5.33	6.02	0.0023
200	20.09	7.87	2.09	1.28	11.489

From this table we can also say that the value of complex modulus relaxation time ($\tau_{M''}$) is less than that of complex impedance relaxation time ($\tau_{Z''}$). The three relaxation times ($\tau_{\tan\delta}$, $\tau_{Z''}$, $\tau_{M''}$) follow the order given below:

$$\tau_{\tan\delta} > \tau_{Z''} > \tau_{M''}$$

The relaxor behavior as observed in these ceramics can be induced by many reasons, such as microscopic composition fluctuation, the merging of micropolar regions into macropolar regions, or a coupling of order parameter and local disorder mode through the local strain [32]. As no macroscopic phase separation exists in the studied ceramic, we cannot exclude chemical heterogeneity in nanoscale. It is also clear from Fig. 10 that M′(ω) shows a dispersion behavior at higher frequency tending towards M_∞ (M_∞ = the asymptotic value of M′(ω) at higher frequencies) while M″(ω) exhibit a maximum (M''_{max}) centered at dispersion region of M′(ω). The temperature independent nature of superimposed plots between M′/ M'_{max} versus log(f/f_{max}) and M″/ M''_{max} versus log(f/f_{max}) are shown in Fig. 11.

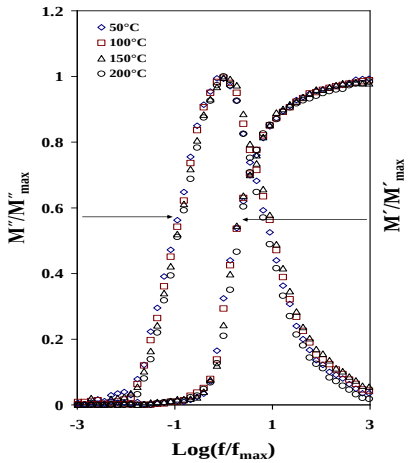

Fig. 11 Variations of M′/M'_{max} and M″/M''_{max} with frequency for BBFO3 sample (T_a = 800°C).

The perfect overlapping of all the curves on a single master curve suggests that the mechanism underlying the dynamic process is temperature independent and conductivity relaxation occurring at different frequencies exhibit temperature independent dynamic processes. This time-temperature superposition shows that conduction mechanism remains unchanged. It indicates a common ion transport mechanism, which operates in the entire range of composition and temperature studied.

IV. CONCLUSIONS

Bismuth layered polycrystalline ceramics $(Bi_2O_3)(Ba_xFe_{1-x}O_3)$ with different compositions ($0.2 \leq x \leq 0.8$, x is in step of 0.2) were prepared by high temperature solid-state reaction method. The X-ray structural study of the samples confirms the single polycrystalline phase. The dielectric properties, such as ε′ and ε″ and their variations with frequency and temperature, indicates dispersion at lower frequency. Significant dielectric enhancement with temperature is observed in all the samples. Electric conductivity increases with increase in Ba ion concentration. Studies of temperature dependent conductivity (ac/dc) suggested that the conduction mechanism is of mixed type (i.e., due to the charge carrier ions and polarons). A significant change in activation energy was observed with frequency and dopant concentration. The ac activation energies increased with increase in Ba ion concentration. From the impedance spectroscopic studies, the samples showed relaxational effects. All the samples show a NTCR behavior in the studied range of temperature and frequency. Appearance of Debye like peak in Z″ vs f plots indicates the presence of space charge accumulation. The occurrence of master curve of electric modulus at all the temperatures in the investigated ceramics indicates that the mechanism underlying the dynamic process is temperature independent.

REFERENCES

[1]. Aurivillius B 1949a Ark. Kemi **1** 463.
[2]. Aurivillius B 1949b Ark. Kemi **1** 499.
[3]. C. A. P. de Arauzo, J. F. Scott, Science 246 (1989) 1400.
[4]. D. L. Sidebottom, B. Rolling, K. Funke, Phys. Rev. B 63 (2000) 024301.

[5]. A. K. Singh, T. C. Goel, R. G. Mendiratta, O. P. Thakur, C. Prakash, J. Appl. Phys. 91 (2002) 6626.
[6]. N. Sivakumar, A. Narayanasamy, N. Ponpandian, G. Govindaraj, J. Appl. Phys. 101 (2007) 084116.
[7]. S. Ezhilvalavan, J.M. Xue, J. Wang, Mater. Chem. Phys. 75(1–3) (2002) 50.
[8]. A. Moguš-Milanković, A. Šantić, M. Karabulut, D. E. Day, J. Non-Cryst. Solids 330 (2003) 128.
[9]. G. A. Smolenskii, V. A. Bokov, V. A. Isupov, N. N. Krainic, R. E. Posynkov and A. I. Sokolov, Ferroelectrics and related materials, Gordon and Breach, NY, 696 (1984).
[10]. T. K. Li, Y. Zhu, S. B. Desu, C. Peng, M. Nagata, Appl. Phy. Lett. 86 (1996) 29.
[11]. N. V. Prasad, Mahendra Kumar, G. Prasad, T. Bhimasankaran, S. V. Suryanarayana, G. S. Kumar, Bull. Mater. Sci. 23 (2000) 483.
[12]. E. C. Subba Rao, J. Phys. Chem. Solids 23 (1962) 665.
[13]. T. Takenaka, K Sakata, Jap. J. Apply. Phys. 19 (1980) 31.
[14]. A. Srinivas, M. Mahesh Kumar, S. V. Suryanarayana, T. Bhimasankaram, Mater. Res. Bull. 34(6) (1999) 989.
[15]. A. Srinivas, S.V. Suryanarayana, G.S. Kumar, M. Mahesh Kumar, J. Phys.: Condens. Matter 11, (1999) 3335.
[16]. A. Chen, Y. Zhi, and L. E. Cross, Phy. Rev. B 62 (2000) 228.
[17]. C. H. Lu, C. Y. Wen, Mater. Lett. 38 (1999) 278.
[18]. B. A. Boukamp, J. Electrochem. Soc. 142 (1995) 188.
[19]. Y. Zhi, A. Chen, P. M. Vilarinho, and J. L. Baptista, J. Appl. Phy. 83, (1998) 4874.
[20]. R. Waser, J. Am. Ceram. Soc. 74 (1991) 1934.
[21]. X.F. Du, I.W. Chen, J. Am. Ceram. Soc. 81 (1998) 3253.
[22]. S.K. Patri, R.N.P. Choudhary, B.K. Samantaray, J. Alloys Compd. 459 (2008) 333.
[23]. C.M. Wanga, J.F. Wang, Appl. Phys. Lett. 89 (2006) 202905.
[24]. R. Gerhardt. J. Phys. Chem. Solids 55 (1994) 1491.
[25]. F. S. Howell, R. A. Bose, P. B. Macedo, C. T. Moynhan, J. Phys. Chem. 78 (1974) 639.
[26]. S.K. Patri, R.N.P. Choudhary, B.K. Samantaray, J. Electroceram. 20 (2008) 119.
[27]. S.K. Patri, R.N.P. Choudhary, Cent. Eur. J. Phys. doi:10.2478/S11534-008-0064-7, (2008)
[28]. S. Allen, E. Thomas, The Structure of Materials (Wiley, New York, 1999).
[29]. G. Catalan, B. Noheda, J. McAneney, I. J. Sinnamon, J.M. Gregg, Phys. Rev. B 72 (2005) 020102.
[30]. G.K. Williamson, W.H. Hall, Acta Metall. 1 (1953) 22.
[31]. R.N.P. Choudhary, D.K. Pradhan, G.E. Bonilla, R.S. Katiyar, J. Alloys Compd. 437 (2007) 220.
[32]. B. E. Vugmeister and M. D. Glinchuk, Rev. Mod. Phys. 62, (1990) 993.